Original Research Article

Modelling and simulation of the earth-to-air heat exchanger in laminar air flow regime for the passive cooling of buildings

ABSTRACT

The earth-to-air heat exchanger is a very energy efficient system for preheating and cooling premises, which consists of circulating air through a tube buried at a certain depth in the ground. The temperature of the ground is less variable than that of the outside air, so that the air leaving the exchanger is more temperate. In the warm periods of the year, the air is cooled while it is warmed during the cold periods. The present work is devoted to the modelling and numerical simulation of the mixed convection earth-to-air heat exchanger in laminar regime. The mixed convection equations governing the heat transfers in the earth-to-air heat exchanger and in the building as well as the boundary and initial conditions have been presented and discretized using the finite difference method with an Alternate Direction Implicit (ADI) scheme. The linear algebraic equations obtained are solved using the Thomas algorithm combined with an iterative Gauss-Seidel procedure. The results show that the flow is dominated by forced convection. The analysis of the effect of Reynolds number indicated that the temperature, average Nusselt number and earth-to-air heat exchanger efficiency increase with Reynolds number.

Keywords: Laminar regime, Canadian well, earth-to-air heat exchanger, heat transfer, soil temperature

1. INTRODUCTION

Buildings account for a significant proportion of household electricity bills and contribute to greenhouse gas emissions through the use of air conditioners and evaporative coolers for heating and cooling buildings [1]. In order to reduce energy consumption and achieve thermal comfort inside buildings, sustainable solutions have been explored through the use of passive techniques [2-4]. The earth-to-air heat exchanger system is one of the passive technologies used for heating and cooling of buildings. Li et al [5] conducted a study to explore the potential of applying air-to-ground heat exchanger to preheat fresh air in very cold regions. A double layer earth-to-air heat exchanger and a heat recovery unit were combined to take on the heating load. The performance of the earth-to-air heat exchanger was studied. They carried out experiments between 4 January and 20 April 2017 (local heating season), focusing mainly on variations in air temperature, air flow rate, heating capacity and ground temperature. They found that the earth-to-air heat exchanger could provide an average temperature rise of 12.4 °C in the heating condition. Diaz-Hernandez et al [6] presented an experimental study of an earth-to-air heat exchanger under hot and humid climatic conditions in Mexico. The earth-to-air heat exchanger operated as a cooler during the day and as a heater at night, except during the winter season when it operated mostly as a heater. The earth-to-air heat exchanger generated a temperature difference of 5.5°C as a cooler. The maximum energy withdrawn as a chiller was 4,438 kWh for the month of August. The results show that with the earth-to-air heat exchanger it is possible to cool an

air stream in hot and humid weather conditions. Experiments were carried out by Sakhri et al [7] to study the efficiency of an air-to-ground heat exchanger without external devices (fans, air blowers, etc.) under the climatic conditions of the Bechar region, which is located in southwest Algeria. An increase of 19% in the relative humidity of the earth-to-air heat exchanger was observed in the humidification regime. While a decrease of 27% in relative humidity was achieved in the dehumidification regime. For the humidity regime, the daily working regime was 62.5% dehumidification (from 00:00 to 09:00 and 18:00 to 23:00) and 37.5% humidification (from 10:00 to 17:00). The results show that the earth-to-air heat exchanger technique has an excellent potential for improving the humidity of buildings in arid regions. An experimental study of the energy performance of an underground air tunnel system for cooling greenhouses was carried out by Ozgener et al [8]. This study highlighted the energy performance characteristics of an underground air tunnel for greenhouse cooling. The maximum daily values of the coefficient of performance (COP) of the cooling system are 15.8. The average total COP during the experimental period is 10.09. The overall energy efficiency value of the system on a product/fuel basis is 60.7%. Wu et al [9] carried out experimental measurements and 3D numerical simulations of ground source heat pump systems in a UK climate. The measured thermophysical properties of the soil in situ were used in the Computational Fluid Mechanics (CFM) model. Numerical prediction showed that there was no significant difference in the specific heat extraction by the heat pump for different pipe diameters in the ground. However, the larger the coil diameter, the higher the heat extraction per metre of pipe. The specific heat extraction also increases, but the heat extraction per metre of pipe decreases with increasing distance from the centre gap of the coil. The achievable energy performance using an earth-to-air heat exchanger for building cooling was evaluated during winter and summer by Ascione et al [10]. They developed dynamic simulation codes for the energy performance of buildings. The energy requirements of the systems are analysed for different Italian climates, depending on soil typology, tube material, tube length and depth, air velocity through the tube, ventilation rates and control modes. The earth-to-air heat exchanger is efficient in both winter and summer.

The modelling of earth-to-air heat exchanger (Canadian or provincial wells) requires a good understanding of the principle of their operation, the physical phenomena, the operating parameters that influence the efficiency of earth-to-air heat exchangers.

The literature review shows that much experimental, analytical and numerical work has been done on earth-to-air heat exchangers. However, more work is needed to better understand the physical phenomena that take place in earth-to-air heat exchanger and the many parameters on which the design of these geothermal systems depends on. The present study consists in modelling the heat transfers in the soil and the earth-to-air heat exchanger by taking into account laminar air flow regime in the tube, the depth of burial of the tubes, the length of the tubes, the air inlet velocity expressed from the Reynolds number or the air flow rate, the climatic conditions of Lome, capital of Togo.

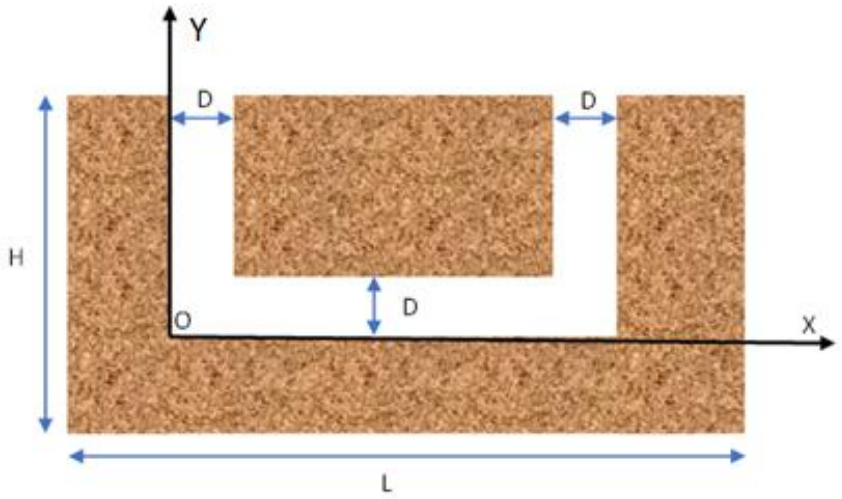

Figure 1. Earth-to-air heat exchanger physical model

2. MODEL CONFIGURATION AND GOVERNING EQUATIONS

2.1. Physical Model

The system subject to study in the present work is an earth-to-air heat exchanger. It is a buried U-shaped tube at a depth H through which air flows. This tube has a length L and a diameter D. The air enters the tube through the left opening with an ambient temperature Ta and a velocity U_0. The geometry of the system is shown in Figure 1. The eath-air heat exchanger is divided into three compartments. The left vertical column of the exchanger where the air enters into the tube is refered to compartment 1, the horizontal part of the exchanger as compartment 2 and the right vertical column leading to the eath-air heat exchanger exit as compartment 3.

2.2. Governing equations in the buried U-shaped tube

2.2.1. Assumptions

To simplify the formulation of the physical problem, the following assumptions are made:

- the flow is assumed to be two-dimensional;
- the fluid is Newtonian and incompressible;
- the flow regime is considered to be laminar;
- heat transfer by radiation is negligible;
- the viscous dissipation and the pressure term in the heat equation are negligible;
- the Boussinesq approximation is valid

2.2.2. Transfer equations

Under the above assumptions, the dimensionless equations in terms of vorticity Ω, temperature θ, concentration C and stream function Ψ governing the studied problem are equations:

$$\frac{\partial \Omega}{\partial \tau} + U\frac{\partial \Omega}{\partial X} + V\frac{\partial \Omega}{\partial Y} = \frac{1}{Re}\left[\frac{\partial^2 \Omega}{\partial X^2} + \frac{\partial^2 \Omega}{\partial Y^2}\right] + Ri_T\frac{\partial \theta}{\partial X} + Ri_M\frac{\partial C}{\partial X} \quad \#(1)$$

$$\frac{\partial \theta}{\partial \tau} + U\frac{\partial \theta}{\partial X} + V\frac{\partial \theta}{\partial Y} = \frac{1}{RePr}\left(\frac{\partial^2 \theta}{\partial X^2} + \frac{\partial^2 \theta}{\partial Y^2}\right) \quad \#(2)$$

$$\frac{\partial C}{\partial \tau} + U\frac{\partial C}{\partial X} + V\frac{\partial C}{\partial Y} = \frac{1}{ScRe}\left(\frac{\partial^2 C}{\partial X^2} + \frac{\partial^2 C}{\partial Y^2}\right) \quad \#(3)$$

$$\frac{\partial^2\Psi}{\partial X^2}+\frac{\partial^2\Psi}{\partial Y^2}=-\Omega\ ;\ U=\frac{\partial\Psi}{\partial Y}\ ;\ V=-\frac{\partial\Psi}{\partial X}\ \#(4)$$

Where $\left(Ri_T=\frac{Gr_T}{Re^2}\right)$ and $Ri_M=\frac{Gr_M}{Re^2}$ are respectively thermal and mass Richardson numbers ; $\left(Gr_T=\frac{g.\beta_T.\Delta T.L^3}{\nu^2}\right)$ and $\left(Gr_M=\frac{g.\beta_M.\Delta C.L^3}{\nu^2}\right)$ are respectively thermal and mass Grashof numbers ; $Re=\frac{\mathrm{V_{in}}L}{\nu}$ is Reynolds number ; $Pr=\nu/\alpha$ is Prandtl number ; $Sc=\frac{\mu}{\rho D}$ is Schimidt number

The employed dimensionless variables used in the governing equations are :

$$\mathrm{X}=\frac{\mathrm{x}}{\mathrm{H}}\ ;\ \mathrm{Y}=\frac{\mathrm{y}}{H}\ ;\ \mathrm{U}=\frac{\mathrm{u}}{\mathrm{V_{in}}};\ \mathrm{V}=\frac{\mathrm{v}}{\mathrm{V_{in}}};\ \tau=\mathrm{t}\frac{\mathrm{V_{in}}}{H};\theta=\frac{\mathrm{T}-\overline{\mathrm{T}}_{soil}}{\overline{\mathrm{T}}_{in}-\overline{\mathrm{T}}_{soil}};\ \mathrm{C}=\frac{\mathrm{c}-\mathrm{c_{in}}}{\overline{\mathrm{c}}_{tube}-\mathrm{c_{in}}};$$

$$\Psi=\frac{\psi}{H\mathrm{V_{in}}};\ \Omega=\frac{\omega H}{\mathrm{V_{in}}}\ \#(5)$$

With $\mathrm{V_{in}}$, $\overline{T}_{in}$, C_{in} are inlet values of velocity, average temperature and vapour concentration. $\overline{\mathrm{T}}_{\mathrm{soil}}$ is the soil avreage temperature and $\overline{\mathrm{c}}_{tube}$ is internal face of the tube average moisture.

2.2.3. Boundary conditions

The dimensionless boundary conditions as indicated in equations (11) to (19) are shown below:

- at the inlet of earth-to-air heat exchanger : $0\le X\le\frac{D}{H}$, $Y=1$

$$U=0;\ V=-1\ ;\ \theta=\theta_{amb};\ C=0;\ \left.\frac{\partial\Psi}{\partial X}\right|_{Y=1}=1;\ \Omega=-\left.\frac{\partial U}{\partial Y}\right|_{Y=1}\ \#(6)$$

- at the outlet of earth-to-air heat exchanger : $\frac{L-D}{H}\le X\le\frac{L}{H}$, $Y=1$

$$\left.\frac{\partial\mathrm{U}}{\partial Y}\right|_{Y=1}=0;\ \left.\frac{\partial\mathrm{V}}{\partial Y}\right|_{Y=1}=0;\ \left.\frac{\partial\theta}{\partial Y}\right|_{Y=1}=0;\ \left.\frac{\partial\mathrm{C}}{\partial Y}\right|_{Y=1}=0;\ \left.\frac{\partial\Psi}{\partial Y}\right|_{Y=1}=0;\ \left.\frac{\partial\Omega}{\partial Y}\right|_{Y=1}=0\ \#(7)$$

- on the left vertical wall of compartment 1 : $X=0$; $0\le Y\le 1$

$$U=U=0;\ \theta=\theta_{soil};\ C=1\ ;\ \Psi=-\frac{D}{H};\ \Omega=\left.\frac{\partial\mathrm{V}}{\partial X}\right|_{X=0}\ \#(8)$$

- on the right vertical wall of compartment 1 **:** $X=\frac{D}{H}$; $\frac{D}{H}\le Y\le 1$

$$U=U=0;\ \theta=\theta_{soil};\ C=1;\ \Psi=0;\ \Omega=\left.\frac{\partial\mathrm{V}}{\partial X}\right|_{X=\frac{D}{H}}\ \#(9)$$

- on the lower horizontal wall of compartment 2 : $0\le X\le\frac{L}{H}$, $Y=0$

$$U=U=0;\ \theta=\theta_{soil};\ C=1;\ \Psi=-\frac{D}{H};\ \Omega=-\left.\frac{\partial\mathrm{U}}{\partial Y}\right|_{Y=0}\ \#(10)$$

- on upper horizontal wall of compartment 2 : $\frac{D}{H}\le X\le\frac{L-D}{H}$, $Y=\frac{D}{H}$

$$U=V=0\ ;\ \theta=\theta_{soil};\ C=1;\ \Psi=0;\ \Omega=-\left.\frac{\partial\mathrm{U}}{\partial Y}\right|_{Y=\frac{D}{H}}\ \#(11)$$

- on the left vertical wall of compartment 3 **:** $X=\frac{L-D}{H}$; $\frac{D}{H}\le Y\le 1$

$$U=U=0\ ;\ \theta=\theta_{soil}\ ;\ C=1\ ;\ \Psi=0;\ \Omega=\left.\frac{\partial\mathrm{V}}{\partial X}\right|_{X=\frac{L-D}{H}}\ \#(12)$$

- on the right vertical wall of compartment 3 : $X=\frac{L}{H}$; $0\le Y\le 1$

$$U=U=0\ ;\ \theta=\theta_{soil}\ ;\ C=1;\ \Psi=-\frac{D}{H}\#(13)$$

2.3. Heat conservation equation in the soil

In the study of the earth-to-air heat exchanger the soil is considered as a semi-infinite medium. In this condition, the heat equation of the soil can be written as :

$$\frac{\partial T_{soil}}{\partial t} = \alpha_{sol} \frac{\partial^2 T_{soil}}{\partial y^2} \ \#(14)$$

The boundary conditions are as follow :

$$T_{soil}(0,t) = T_0 + A_T Cos\ [\omega(t - t_0)]\ ;\ T_{soil}(\infty,t) = T_0 \#(15)$$

with :

$$T_0 = \frac{T_{min}+T_{max}}{2}\ ;\ A_T = \frac{T_{max}-T_{min}}{2}\ \#(16)$$

The analytical solution of this equation is given as [11]:

$$T_{Soil}(z,t) = T_0 + A_T exp\left(-z\sqrt{\frac{\omega}{2\alpha_{sol}}}\right).cos\left(\omega(t - t_0) - z\sqrt{\frac{\omega}{2\alpha_{sol}}}\right) \quad (17)$$

with $Z = H - y$.

2.4. Heat transfer intensity

To characterize -to-ground heat exchanger the intensity of heat transfer between the earth-to-air heat exchanger, the local and average Nusselt number are calculated as follows :

- Local Nusselt number

$$Nu = \frac{H}{\Delta T}\left[\left.\frac{\partial T}{\partial y}\right|_{y=0} + \left.\frac{\partial T}{\partial y}\right|_{z=D} + \left.\frac{\partial T}{\partial x}\right|_{x=0} + \left.\frac{\partial T}{\partial x}\right|_{x=D} + \left.\frac{\partial T}{\partial x}\right|_{x=L}\right] \#(18)$$

- Average Nusselt number

$$\overline{Nu} = \frac{H}{\Delta T}\left[\frac{1}{L}\int_0^L \left.\frac{\partial T}{\partial y}\right|_{y=0} dx + \frac{1}{L-2D}\int_D^{L-D} \left.\frac{\partial T}{\partial y}\right|_{y=0} dx + \frac{1}{H}\int_0^H \left.\frac{\partial T}{\partial x}\right|_{x=0} dy + \frac{1}{H-D}\int_D^H \left.\frac{\partial T}{\partial x}\right|_{x=L} dy + \frac{1}{H}\int_0^H \left.\frac{\partial T}{\partial x}\right|_{x=L} dy\right] \quad (19)$$

2.5. Eath-air heat exchanger efficiency

The earth-to-air heat exchanger determines the performance of the eath-air heat exchanger. It is defined as :

$$E = \frac{\overline{T}_{out} - \overline{T}_{in}}{\overline{T}_{soil} - \overline{T}_{in}} \ \#(20)$$

with :

T_{out}: The average temperature at the outlet of the earth-to-air heat exchanger

T_{in}: Average temperature at the inlet of the earth-to-air heat exchanger

$\overline{T}_{soil}$: Average temperature of the soil at the earth-to-air heat exchanger burial depth

3. NUMERICAL METHOD AND VALIDATION

3.1 Numerical method

The governing equations are discretized by using the finite difference method. The discretized equations are iteratively solved using an alternating direction implicit (ADI) scheme. The system of algebraic equations is solved iteratively by means of the Thomas algorithm. Convergence of the numerical code is established according to the following criterion:

$$\left|\frac{\sum_{i,j=1}^{i_{max},j_{max}} \phi_{i,j}^{n+1} - \sum_{i,j=1}^{i_{max},j_{max}} \phi_{i,j}^{n}}{\sum_{i,j=1}^{i_{max},j_{max}} \phi_{i,j}^{n+1}}\right| \leq 10^{-6} \#(21)$$

where ∅ denotes a dependent variable Ω, Ψ, U, V and θ , the indices i and j indicate the grid positions, and n represents the iteration number. To ensure the convergence of the iterative process, a sub-relaxation coefficient of 0.8 was used.

3.2 Grid independency

In order to choose the size of the grid, accuracy tests using the finite different method for mesh sensitivity analysis were performed for D=0.4 m, L=5 m, H=1 m, Ra=105, Ri=10 and Pr=0.72. Six sets of grids are considered: 151x101, 171x121, 191x141, 201x181, 211x191 and 221x201. The change in stream function and temperature values with the increase of the cells number is reported in Table 1. Reasonably good agreement was found between the grids 201x181 and 211x191. Therefore, to further study, the grid 201x181 with lower cells was considered.

Table 1. Acuracy test for D=0.4 m, L=5 m, H=1 m, Ra=105, Ri=10 and Pr=0.72

Nodes	φ(0.2,0.7)	T(0.2,0.7)
151x101	-0.00321	303.049
171x121	-0.00412	303.043
191x141	-0.00108	303.055
201x181	-0.00115	303.056
211x191	-0.00116	303.057
221x201	-0.00149	303.044

3.3 Validation

To ensure the accuracy of the results of the present numerical scheme, it was validated against the numerical results obtained by Aydin et al [12]. They studied numerically the transport mechanism of laminar mixed convection in a shear and buoyancy driven cavity having a locally heated lower wall and moving cooled sidewalls. The comparison of the numerical results obtained was made concerning the streamlines (Figure 2a) and isotherms (Figure 2b). As can be seen in these figures, there is excellent agreement between the present work and the results obtained by Aydin et al [12]. The variation of local Nusselt number at the heated wall versus x coordinate of this work and that of Aydin et al [12] are also compared (figure 3). It is found that the results are well overlapped. The difference in results is less than 5%. Therefore, the local Nusselt number of the present study agree well with that of Aydin et al [12].

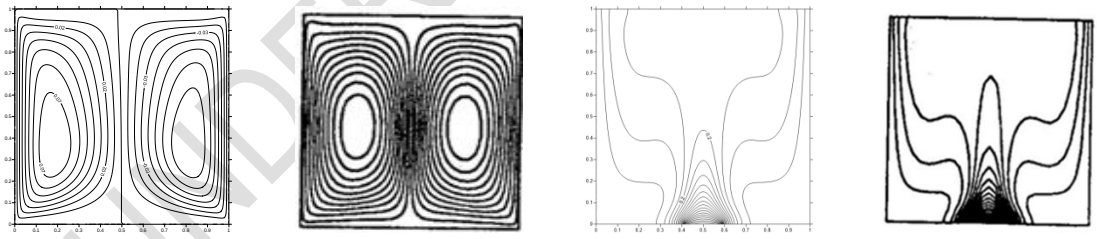

Present work Aydin et al [12] Present work Aydin et al [12]

(a) Streamlines (b) isothermes

Figure 2. Comparison of streamlines and isotherms between the present numerical results and that of Aydin et al [12] for $\varepsilon = \frac{1}{5}$, Re=100 and Ri=10.

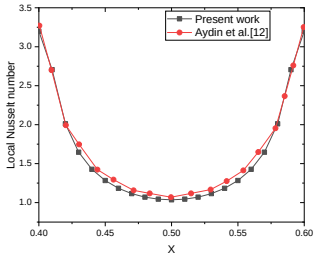

Figure 3. Comparison of streamlines and isotherms between the present numerical results and that of Aydin et al [12] for $\varepsilon = \frac{1}{5}$, Re=100 and Ri=10.

4. RESULTS AND DISCUSSION

In this section, numerical results are presented for the streamlines, isotherms, isoconcentration of vapour, velocity, temperature and vapour concentration profiles, for various values of the Reynolds number and different types of soil. In addition, the average Nusselt numbers and the efficiency of earth-to-air heat exchanger have been calculated.

4.1. Flow fields

Figure 4 shows plots of streamlines for different values of Reynolds number range from 300 to 900. The flow structure is composed of open streamlines (Figure 4a, b and c). These lines originate at the inlet of the exchanger, follow the shape of the U-tube and end at the outlet of the earth-to-air heat exchanger. The open lines observed show that the flow is dominated by forced convection. The absence of recirculation indicates that the natural convection generated by the temperature difference between the air and the tube walls at ground temperature is negligible.

To better understand the flow structure, the profiles of the u and v components of the flow velocity have been presented in Figures 5 and 6. Figure 5 shows that the shape of the u component of the velocity changes from one section of the tube to another. In the left vertical column of the earth-to-air heat exchanger, close to the inlet, the change in the sign of u indicates that the fluid is deflected to the right by the left vertical wall and to the left by the right vertical wall, forcing the fluid to occupy the entire upper part of compartment 1. In the progression of the air flow towards the bottom of the exchanger indicated by the negative sign of the component v of the velocity (Figure 6), the component u becomes positive and shows that the flow approaches the right vertical wall of compartment 1 and starts the first turn into the left bend. In the horizontal part of the tube the positive value of u indicates that the flow is moving towards the right bend and starts the second turn in the right bend. The positive values of v in compartment 3, show that after the turn the flow is ascending and heading towards the exit. These profiles corroborate with the observations made at the open streamlines occupying the entire volume of the U-shape of the tube.

The analysis of the streamline distribution under the influence of the Reynolds number (Figure 4) indicates that the distribution of streamlines is not affected by the variation of the Reynolds number. However, the influence of this parameter on the velocity component profiles in all sections of the earth-to-air heat exchanger is very noticeable (Figure 5 and 6). It can be seen that when the Reynolds number increases, the velocity values increase as a result of the intensification of the forced convection in the channel.

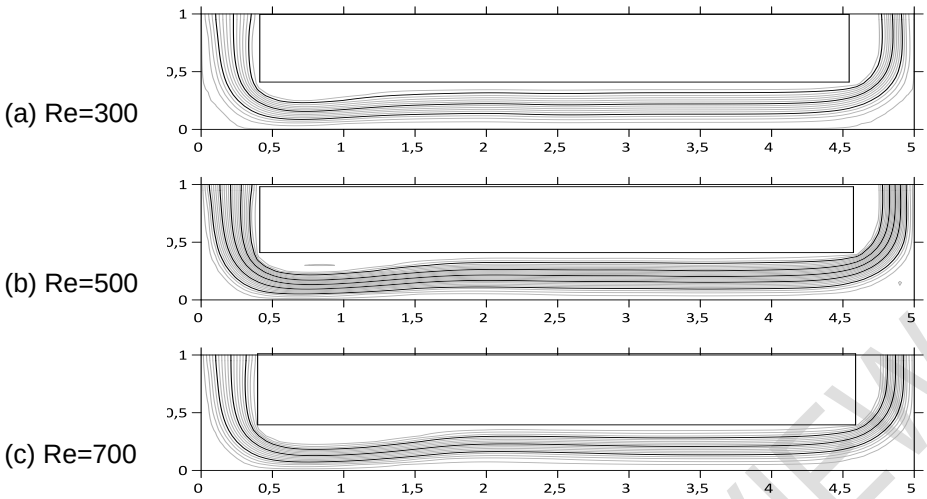

Figure 4. Streamline distribution under the influence of Reynolds number; L= 5m; D=4m; H=1m

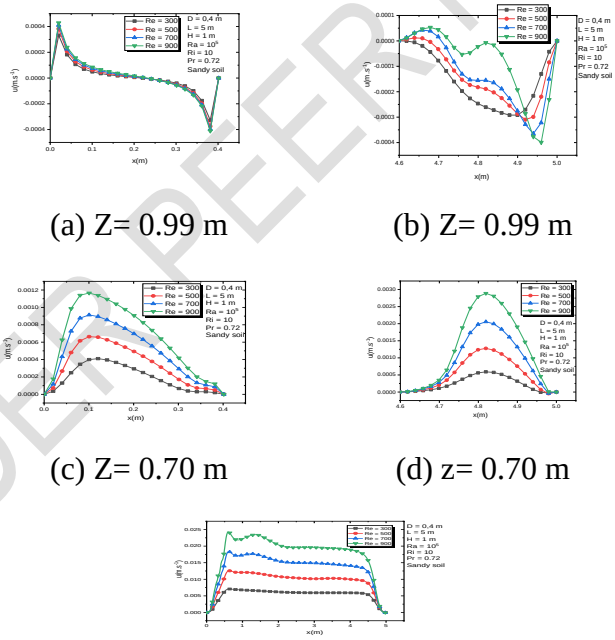

Figure 5. Profiles of the u component of the velocity as a function of the abscissa x in the earth-to-air heat exchanger under the influence of the Reynolds number

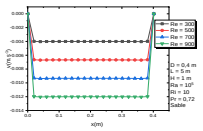

(a) Z= 0.99 m

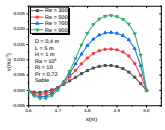

(b) Z= 0.99 m

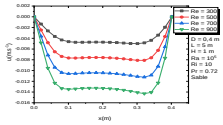

(c) Z= 0.70 m

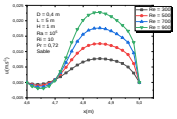

(d) z= 0.70 m

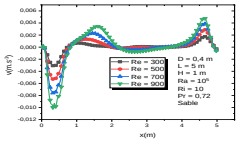

(e) z= 0.20 m

Figure 6. Profiles of the velocity component v as a function of x in the earth-to-air heat exchanger under the influence of the Reynolds number

4.2 Temperature fields

Figure 7 shows the distribution of isotherms in the earth-to-air heat exchanger. The isotherm lines have a lanceolate shape with wide bases and the tip pointing in the direction of flow. As with the streamlines, these isotherms become deformed at the bends and take on the shape of a "U" shaped tube through which air is flowing. The isotherms tend to be parallel to the walls, indicating heat transfer by convection-conduction between the tube walls and the air. A cell of isotherms is also observed at the right bend of the tube.

The distribution of the isotherms is explained by the temperature profiles shown in Figure 8. This figure shows that the temperature versus x profiles in compartment 1 are similar to parabolas with the vertices pointing in the opposite direction of the flow (Figures 8.a and c). The lowest temperature values are observed in the vicinity of the walls in contact with the ground. The highest values correspond to those of the hot air progressing through the exchanger. In compartment 3, the temperature undergoes a strong variation whose amplitude decreases towards the earth-to-air heat exchanger outlet indicating a cooling of the air (Figures 8.b and d). Figure 7 shows the temperature fields in the earth-to-air heat exchanger channel for different values of Reynolds number. In contrast to the streamline distribution, the isotherms are strongly modified by the influence of the Reynolds number. A lengthening of the consecutive cells is observed as the Reynolds number increases. A cell of isotherms appears in the right corner of the exchanger as a result of the increase in Reynolds number. The impact of the Reynolds number on the temperature values is elucidated in Figure 8. This figure shows the variation of the temperature as a function of x for different Reynolds numbers. It can be seen that as the Reynolds number increases, the temperature increases. The increase of the Reynolds number has the effect of intensifying the transfers by forced convection and thus reduces the residence time of the air in the exchanger. This does not favour its cooling.

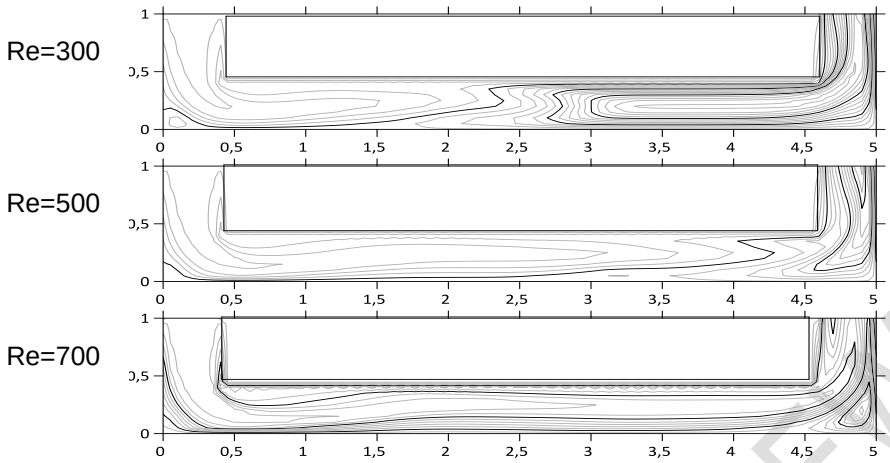

Figure 7. Distribution of isotherms under the influence of Reynolds number; L= 5 m; D=4m; H=1 m

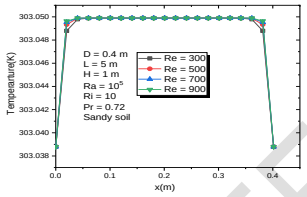

(a) Z= 0.99 m

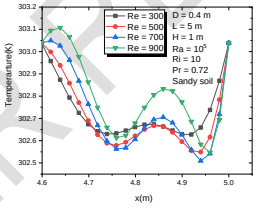

(b) Z= 0.99 m

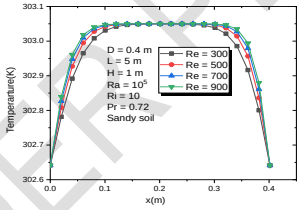

(c) Z= 0.70 m

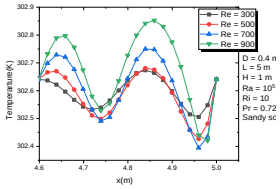

(d) z= 0.70 m

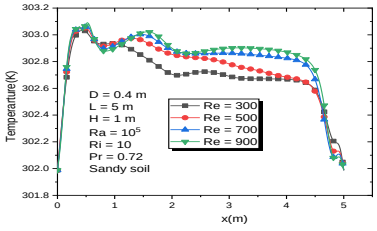

(e) z= 0.20 m

Figure 8: Temperature versus x profiles in the earth-to-air heat exchanger under the influence of Reynolds number

4.3 Heat transfer rate

The Nusselt number (Nu) is a dimensionless number used in heat transfer operations. It represents the ratio of total heat transfer to conductive heat transfer. In order to analyze the heat transfer between the different walls and the adjacent fluid, we have defined an average Nusselt number which is represented as a function of time in figure 9. It can be seen that the average Nusselt number decreases with time. This indicates a decrease in heat transfer over time due to the very small temperature gradient between the walls of the earth-to-air heat exchanger and the air.

The evolution of the Nusselt number can be seen in figure 9 which shows a growth of the mean Nusselt number with the increase of the Reynolds number. Indeed, the increase of the Nusselt number results from the intensification of the convective transfers between the walls of the earth-to-air heat exchanger and the air.

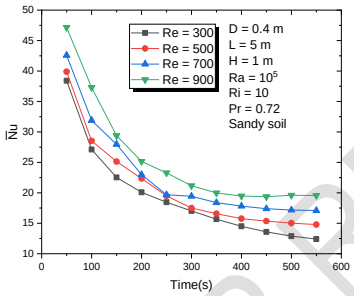

Figure 9: Evolution of the average Nusselt number under the influence of the Reynolds number

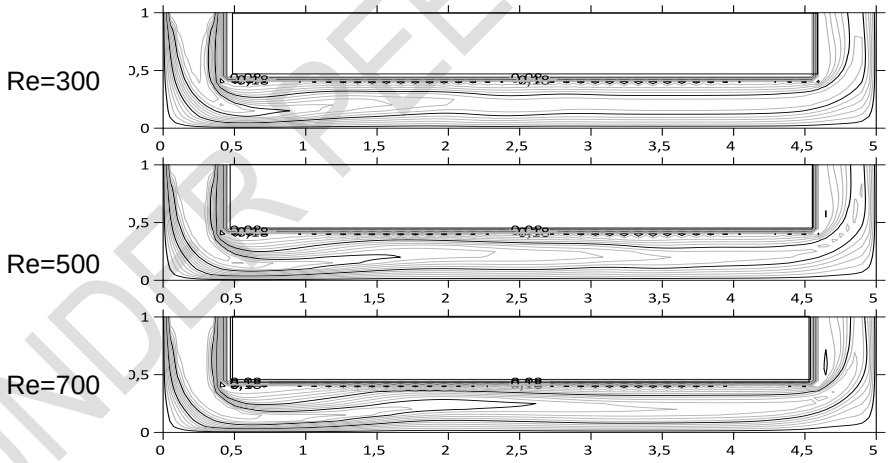

Figure 10: Distribution of humidity isovals under the influence of Reynolds number; L= 5 m; D=4m; H=1 m; Sandy soil.

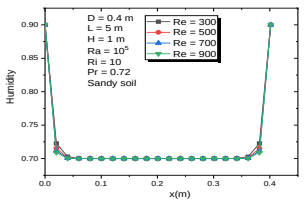

Z= 0.99 m

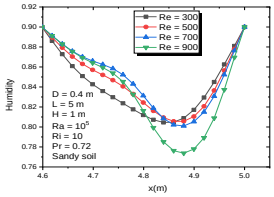

Z= 0.99 m

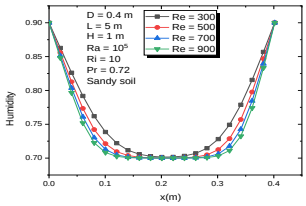

(c) Z= 0.70 m

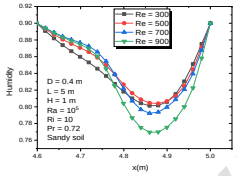

(d) z= 0.70 m

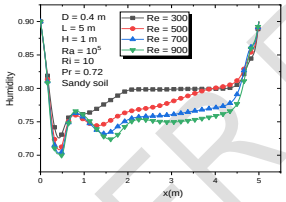

(e) z= 0.20 m

Figure 11: Humidity profiles as a function of x in the air/soil exchanger under the influence of Reynolds number

4.4 Humidity fields

Figure 10 shows that the distribution of humidity isovalues is similar to that of temperature. It is characterized by a succession of lanceolate lines originating at the inlet of the earth-to-air heat exchanger and whose tip is embedded in the main flow. In the vicinity of the walls these lines are very tight and parallel to the walls. This distribution shows that moisture transfer is more intense in these areas.

The moisture profiles presented in figure 11 show that the profiles are parabolic with the peaks pointing in the direction of flow in compartment 1 (Figure 11-a and c) and against the direction of flow in compartment 3 (Figure 11-b and d). The minimum moisture values are observed at the top and the maximum values near the walls.

The influence of the Reynolds number and consequently of the air flow rate at the earth-to-air heat exchanger inlet on the moisture isovalue distribution is shown in Figure 10. This figure shows that when the Reynolds number increases, as in the case of the isotherms, the lanceolate cells become longer and move towards the exchanger outlet. This influence can also be seen in the profiles (Figure 11) where a decrease in humidity is observed as the Reynolds number increases.

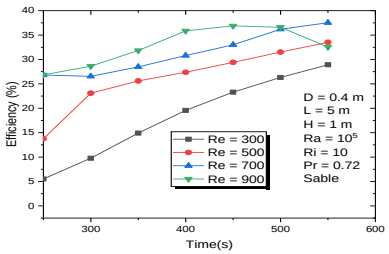

Figure 12. Evolution of the efficiency of the earth-air heat exchanger under the influence of the Reynolds number

4.6 Earth-to-air heat exchanger efficiency

The efficiency of the earth-to-air heat exchanger is shown in figure 12. Examination of this figure shows that the efficiency of the earth-to-air heat exchanger increases with time.
Figure 12 shows also the evolution of the earth-to-air heat exchanger efficiency for a range of Reynolds numbers from 300 to 900. An examination of this figure indicates that the efficiency of the earth-to-air heat exchanger increases with increasing Reynolds number.
The investigation of the influence of the nature of the soil on the evolution of the earth-to-air heat exchanger efficiency is presented in Figure 12. It can be seen in this figure that the values of the earth-to-air heat exchanger efficiency are only slightly influenced by the nature of the soil. Nevertheless, we note a slightly better efficiency for the sandy soil than for the sandy-clayey silt and clayey soils.

5. CONCLUSION

The present numerical study focused on the potential of the passive cooling of buildings by earth-to-air heat exchanger taking into account the laminar air flow regime. The analysis is performed numerically rendering the use of finite difference method. To understand the consequences of the variation of Reynolds number on the fluid flow and heat transfer characteristics inside the U-shaped caviity of the earth-to-air heat exchanger, an in-depth analysis has been carried out by examining the streamlines, isotherms, vapour isoconcentrations and fhe profiles of velocity, temperature, vapour concentration, averaged Nusselt number and earth-to-air heat exchanger efficiency The major outcomes of the present investigation can be summarized as follows :

-the flow structure consists of open flow lines. These lines originate at the inlet of the earth-to-air heat exchanger, follow the shape of the U-tube and end at the outlet of the earth-to-air heat exchanger. The open lines observed show that the flow is dominated by forced convection.
- the isothermal lines have a lanceolate shape with wide bases and the tip pointing in the direction of flow. As with streamlines these isotherms deform at the bends and take on the shape of a 'U' shaped tube through which air flows. The isotherms tend to be parallel to the walls, indicating heat transfer by convection-conduction between the tube walls and the air.
- the average Nusselt number decreases over time in the range of time. This indicates a decrease in heat transfer over time due to the very small temperature gradient between the earth-to-air heat exchanger walls and the air;
- the distribution of humidity isovalues is similar to that of temperature. It is characterised by a succession of lanceolate isolines originating from the earth-to-air heat exchanger inlet and whose tip is embedded in the main flow;
- the efficiency of the exchanger increases with time in the range of time considered;

- the temperature, average Nusselt number and efficiency of the earth-to-air heat exchanger increase with the Reynolds number.

.

REFERENCES

1. Mihalakakou G., Souliotis M., Papadaki M., Halkos G., Paravantis J., Makridis S., Papaefthimiou S. Applications of earth-to-air heat exchangers: A holistic review Renewable and Sustainable Energy Reviews 2022;155: 111921
2. Mihalakakou G, Santamouris M, Asimakopoulos D. Modelling the thermal performance of earth-to-air heat exchangers. Sol Energy 1994;53(3):301–5.
3. Sawhney R, Buddhi D, Thanu N. An experimental study of summer performance of a recirculation type underground air pipe air conditioning system. Build Environ 1999;34:189–96.
4. Vaz J, Sattler MA, dos Santos ED, Isoldi LA. Experimental and numerical analysis of an earthair heat exchanger. Energy Build 2011;43(9):2476–82.
5. Li H, Yu Y, Niu F, Shafik M, Chen B. Performance of a coupled cooling system with earth-to-air heat exchanger and solar chimney. Renew Energy 2014; 62:468–477. http://dx.doi.org/10.1016/j.renene.2013.08.008.
6. Diaz-Hernandez H.P., Macias-Melo E.V., Aguilar-Castro K.M., Hernandez-Perez I., Xaman J., Serrano-Arellano J., Lopez-Manrique L.M. Experimental study of an earth to air heat exchanger (EAHE) for warm humid climatic conditions. Geothermics 2020; 84:101741
   https://doi.org/10.1016/j.geothermics.2019.101741
7. Sakhria N., Mennib Y., Ameurc H. Experimental investigation of the performance of earth-to-air heat exchangers in arid environments. Journal of Arid Environments 2020; 180:104215
   https://doi.org/10.1016/j.jaridenv.2020.104215
8. Ozgener L., Ozgener O. An experimental study of the exergetic performance of an underground air tunnel system for greenhouse cooling. Renewable Energy 2010; 35: 2804-2811
9. Wu Y., Gan G., Verhoef A., Vidale P. L., Gonzalez R. G. Experimental measurement and numerical simulation of horizontal-coupled slinky ground source heat exchangers. Applied Thermal Engineering 2010: 302574-258.
   doi:10.1016/j.applthermaleng.2010.07.008
10. Ascione F., Bellia L., Minichiello F. Earth-to-air heat exchangers for Italian climates. Renewable Energy 2011; 36:2177-2188.
11. Kolani Y.; Aoukou K. D. D., N'wuitcha K., Banna M. Analytical and numerical studies of transient heat transfer in Soil for geothermal systems. Physical Science International Journal 2022. 26(4): 17-33.
12. Aydin O., Yang W.J. Mixed convection in cavities with a locally heated lower wall and moving sidewalls, Numerical Heat Transfer, Part A: Applications: An International Journal of Computation and Methodology 2000: 37(7): 695-710.
    http://dx.doi.org/10.1080/104077800274037.

NOMENCLATURE

Symbol Description

c	dimensionless moisture
C	dimensional moisture (%)
C_{in}	inlet moisture (%)
$\overline{c}_{tube}$	is internal face of the tube average moisture
D	diameter of the buried tube (m)
E	eath-air heat exchanger efficiency (%)

Gr_T	thermal Grashof number $\left(Gr_T = \frac{g.\beta_T.\Delta T.L^3}{\nu^2}\right)$
Gr_M	mass Grashof number $\left(Gr_M = \frac{g.\beta_M.\Delta C.L^3}{\nu^2}\right)$
H	depth of the earth-to-air heat exchanger
L	length of horizontal part of buried tube
Nu	local Nusselt number
$\overline{Nu}$	average Nusselt number
Pr	Prandtl number $(Pr = \nu/\alpha)$
Re	Reynolds number $\left(Re = \frac{V_{in}L}{\nu}\right)$
Ri_T	thermal Richardson number $\left(Ri_T = \frac{Gr_T}{Re^2}\right)$
Ri_M	mass Richardson number $\left(Ri_M = \frac{Gr_M}{Re^2}\right)$
Sc	Schmidt number $\left(Sc = \frac{\mu}{\rho D}\right)$
t	dimensional (s)
T	dimensional air temperature in the tube (K)
$\overline{T}_{in}$	inlet air average temperature (K)
T_{min}	minimum average temperature of the year (K)
T_{max}	maximum average temperature of the year (K)
T_{out}	average temperature at the outlet of the exchanger (K)
T_{soil}	soil temperature (K)
$\overline{T}_{soil}$	soil average temperature (K)
u	dimensional velocity component in x-direction $(m.s^{-1})$
U	non-dimensional velocity component in X-direction
v	dimensional velocity component in y-direction $(m.s^{-1})$
V	non-dimensional velocity component in Y-direction
V_{in}	inlet velocity $(m.s^{-1})$
x	cartesian coordinate in horizontal direction (m)
X	non-dimensional coordinate in horizontal direction
y	cartesian coordinate in vertical direction (m)
Y	non-dimensional coordinate in vertical direction

Greek Symbols

α	air thermal diffusivity $(m^2.s^{-1})$
α_{soil}	soil thermal diffusivity $(m^2.s^{-1})$
θ	non-dimensional air temperature in the tube
θ_{soil}	non-dimensional soil temperature
ψ	stream function $(m^2.s^{-1})$
Ψ	dimensionless stream function
ω	dimensional vorticity (s^{-1})
Ω	dimensionless vorticity
τ	dimensionless time
μ	dynamic viscosity $\left(k_g.m^{-1}.s^{-1}\right)$
ν	cinematic viscosity $(m^2.s^{-1})$
ρ	density $(kg.m^{-3})$

Subscripts

in	inlet
M	mass
min	minimum
max	maximum
out	outlet
soil	relative to the soil
T	thermal

tube relative to the tube